

# Optical and electronic characteristics of single walled carbon nanotubes and silicon nanoclusters by terahertz spectroscopy

Hakan Altan, Feng Huang, and John F. Federici

*Department of Physics, New Jersey Institute of Technology, Newark, New Jersey 07102*

Aidong Lan and Haim Grebel

*Electronic Imaging Center at NJIT and the Department of Electrical and Computer Engineering, New Jersey Institute of Technology, Newark, New Jersey 07102*

(Received 17 May 2004; accepted 18 August 2004)

We have conducted visible pump-THz (THz—terahertz) probe measurements on single wall carbon nanotubes deposited on quartz substrates. Our results suggest that the photoexcited nanotubes exhibit localized transport due to Lorentz-type photoinduced localized states from 0.2 to 0.7 THz. Upon modeling the THz transmission through the photoexcited layer with an effective dielectric constant given by Maxwell-Garnett theory we found that the data are best fit by a broad Lorentz state at 0.5 THz. These experiments were repeated for ion-implanted, 3–4 nm Si nanoclusters in quartz for which a similar behavior was observed. © 2004 American Institute of Physics. [DOI: 10.1063/1.1805720]

## I. INTRODUCTION

Single wall carbon nanotubes (SWCNTs) have been extensively studied in recent years owing to their unique optical and electronic characteristics.<sup>1,2</sup> Most growth techniques, employed by many research groups, result in a mixture of semiconductor and metallic tubes. In contrast, our SWCNTs predominantly consist of the semiconductor type, making them suitable candidate materials for carrier-induced applications. Linear and nonlinear optical characterization techniques have been used for SWCNTs in suspension,<sup>3</sup> or embedded in a dielectric host material.<sup>4</sup> Whether they are in dielectric hosts or, directly deposited on a substrate, optical techniques have been used to deduce carrier dynamics of nanocomposites in the visible, near, and mid-IR wavelength region.<sup>5</sup> Although these techniques provide a wealth of information there have been only a few studies in the far-infrared region of the spectrum and, in particular, the terahertz (THz) regime,<sup>6,7</sup> where intraband transitions are expected. This is also true for artificial dielectrics made of CdSe nanoparticles<sup>8</sup> and InP nanoparticle arrays<sup>9</sup> within another host material. THz time domain spectroscopy (THz-TDS) and visible pump-THz probe spectroscopy has been widely used to study ultrafast dynamics of many semiconductors.<sup>10–13</sup> One major advantage of THz spectroscopy is the ability to deduce electronic properties of materials without the necessity to overlay physical contacts making it a “noncontact” technique. Therefore, by probing photoinduced carriers with THz spectroscopy one hopes to directly deduce the electronic mobility in these nanostructures.

In this paper we report on results for the nonlinear response of SWCNT films and ion implanted Si nanocrystals using visible pump-THz probe spectroscopy. The samples exhibited unique differential (pump light on/ pump light off) spectra that can be analyzed to extract their electronic properties. With our experimental setup we were able to scan the response of the samples from 0.2 to 0.7 THz.

## II. METHODOLOGY

Films consisting of SWCNTs were synthesized using a chemical vapor deposition technique at a relatively low temperature of 750 °C. The nanotubes were formed on a quartz substrate in the presence of CO gas using Co particles as a catalyst. It will be shown that the catalyst did not play a role in our measurements. This growth method resulted in predominantly semiconductive nanotubes.<sup>4</sup> The average diameter of the tubes was 0.9 nm. The tubes were distributed over a 2 cm<sup>2</sup> area with a film thickness of less than 100 nm. White light experiments exhibited a large loss at wavelengths shorter than 500 nm.<sup>2</sup> A separate set of samples consists of silicon nanocrystals formed by ion implantation into fused silica substrates. The film thickness was 300 nm and was composed of 3–4 nm Si nanocrystals. The overall thickness of the quartz substrate was 200 μm. Previous white light and photoluminescence measurements<sup>14</sup> exhibited an absorption band around  $\lambda=400$  nm suggesting that the carrier dynamics can be well examined with a visible pump-THz probe technique.

The samples were placed into our THz-TDS system, which can be easily configured for visible pump-THz probe spectroscopy as described below and shown in Fig. 1. The THz pulses were on the order of a few picoseconds. The pulses were generated and detected using low-temperature (LT)-GaAs antennas. These antennas were irradiated by 10 mW, ~100 fs pulses from a Ti:sapphire laser with a center wavelength at  $\lambda=800$  nm. The pulsed THz radiation from the transmitter was collimated and focused down to a spot size of 3 mm onto the back side of the sample surface using a series of parabolic mirrors. The sample was placed at 45° relative to both the pump and probe beams. The visible excitation at  $\lambda=400$  nm and pulse duration of ~100 fs was generated through a second harmonic generator using a 1 mm thick crystal of lithium triborate. The pulses were incident on the front side of the sample with a beam diameter of ~5 mm. The THz probing pulses were transmitted through

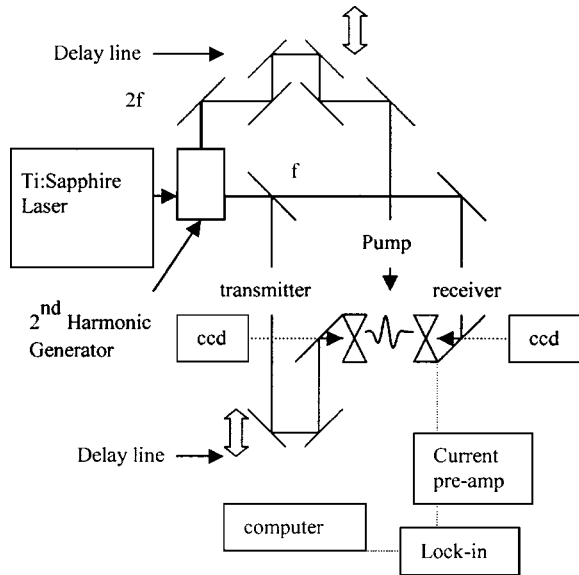


FIG. 1. Visible pump-THz probe spectroscopic configuration. A second harmonic generation module is required to generate blue light for photoexcitation of the nanocomposites.

the sample and then collimated and focused down onto the receiver. The frequency dependent absorption and dispersion of the sample could be obtained with Fourier analysis of the transmitted and reference pulses.<sup>15</sup> In the visible pump-THz probe configuration a dc bias was used and the probing pulse was delayed with respect to the pump pulse. With this configuration, the THz electric field was always measured when the peak pump intensity was incident on the sample. The measured signal was detected by phase-sensitive detection (i.e., lock-in amplifier) techniques, and was referenced to the visible pump beam that was mechanically chopped. Using this differential technique, the measured THz signal was a direct measure of the change in THz transmission through the illuminated (at the peak of illumination) and unilluminated sample.

### III. RESULTS

The THz transmission spectra through unilluminated SWCNTs exhibited an essentially flat spectrum with no significant absorptive features. However, upon visible illumination and the photogeneration of charge carriers, changes in the spectral response of the SWCNT samples were observed. Figures 2(a) and 2(b) shows the response of the transient THz electric field through a SWCNT sample under visible

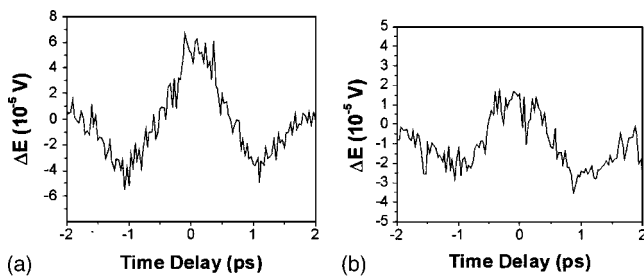


FIG. 2. Differential THz electric field transmission of SWCNTs on quartz substrates. The two curves are taken from two different sample locations.

pumping at  $\lambda=400$  nm with a power level of 30 mW. The two curves of Fig. 2 were taken from two different positions on the sample to effectively study sample inhomogeneity. The  $t=0$  point corresponds to the time at which the peaks of the pumping and THz pulses arrive concurrently on the sample. This  $t=0$  point was determined by time-resolved visible pump-THz probe measurements on a low-temperature grown (LT)-GaAs sample. Multiple visible pump-THz probe scans of the SWCNTs were obtained and then averaged to improve the signal-to-noise ratio. This averaging was required due to the relatively thin layer of the sample. The change in THz transmission is expected to be small due to the relatively low pump power levels ( $<1/100$ ), compared to previous visible pump-visible probe measurements on similar samples.<sup>3</sup> However, we note that the THz probe is inherently more sensitive than the visible probe employed in those measurements

In addition, pump/probe experiments were performed on the substrate with and without the catalyst in order to eliminate the catalyst effects. It was found that the catalyst particles had no absorption features in the THz frequency range. In all of our experiments, the THz center wavelength was much larger than any of the nanoscale features of our samples.

Differential pump/probe experiments with pump power of 30 mW at  $\lambda=400$  nm on ion-implanted silicon embedded in quartz exhibited similar behavior as the SWCNTs [Fig. 3(a)]. Similar to SWCNTs,<sup>16</sup> these samples exhibited fast carrier relaxation time on the order of a few picoseconds.<sup>17</sup> Bulk Si (intrinsic Si wafer with a thickness of 700  $\mu\text{m}$ ) was used as a reference material [Fig. 3(b)]. Again, multiple scans were averaged to improve the signal-to-noise ratio.

In further analysis, the pump power level at  $\lambda=400$  nm was lowered to a level of 20 mW. Ion implanted Si films exhibited a weak but a visible absorption [Fig. 3(a)]; however, the pump power was not high enough to produce a similar time-domain trace.

### IV. ANALYSIS

The presence of noise in the time-domain signals of Figs. 2(a), 2(b), and 3(a) must be considered while computing the Fourier transform of the time-domain data to extract the frequency domain data. Subtle changes in the padding of the data, prior to the Fourier transform algorithm, for example, can lead to large spectral features in the frequency domain. Since the window of data collection is limited in time, zeros are added to the beginning and end of the data set so that its Fourier transform appears smoother and more pronounced. Prior to computing the Fourier transforms, one needs to ensure that no discontinuity was introduced in the time-domain data. The offset of the padding was varied relative to the offset of the raw data to ensure that erroneous spectral features were not introduced. The significant noise contribution to the time-domain signals required special attention to ensure that the corresponding spectral features were not attributable to noise in the time-domain signal. Fine scale time-domain features on the order of 100 fs are noise since the THz detectors are not sensitive to electric field

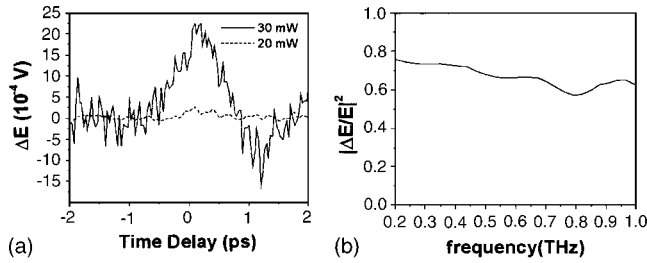


FIG. 3. Ion-implanted Si in a quartz substrate: (a) visible pump-THz probe with visible excitation at  $\lambda=400$  nm and power= $30$  mW/cm<sup>2</sup> (solid line), the dashed line is taken at a pump power of  $20$  mW/cm<sup>2</sup>. (b) Differential transmission under a CW Ar<sup>+</sup>-ion laser ( $\lambda=514$  nm) through bulk silicon for comparison with ion-implanted Si nanocrystals.

fluctuations on this time scale. These fluctuations, therefore, give an estimate of the noise contribution to the THz wave form.

In order to assess the effect of the time-domain noise on the frequency domain spectral features, Fourier transforms of different time-domain data sets, which were consistent with the noise level, were compared. Based on the variation in the Fourier transforms for the SWCNT data over the range of  $0.2$ – $0.7$  THz, the error in the value of  $|\Delta E/E|$  was assessed as  $\approx 20\%$ . A similar analysis suggested that the error in the magnitude of ion-implanted differential spectra was roughly  $30\%$ . Within these noise limits, the SWCNT sample exhibited a broad peak in the  $0.2$ – $0.7$  THz range, while the differential THz spectrum for the ion-implanted silicon sample was essentially flat.

A better understanding of the significance of the differential spectrum of the above nanocomposites can be extracted by analyzing the pump-THz probe spectra using two different transport models: a free-carrier Drude model and a Lorentz model. In the free-carrier Drude model, the frequency dependent dielectric constant of the nanofilm is modeled as

$$\epsilon(\omega) = \epsilon_\infty - \frac{\omega_p^2}{\omega(\omega + i/\tau)}, \quad (1)$$

where  $\epsilon_\infty$  is the dielectric constant of the material at high frequencies,  $1/\tau$  is the collision frequency,  $\omega_p = (4\pi Ne^2/m)^{1/2}$ ,  $N$ ,  $e$ , and  $m$  are the plasma frequency, number density, charge, and mass of the free carriers, respectively. Upon visible excitation, the free-carrier contribution is change by the photoexcitation of free carriers. Previous attempts to fit our data to a Drude model<sup>18</sup> demonstrated that the photoexcited carriers do not exhibit Drude-like transport. In contrast, pump-THz probe measurements of a CdSe nanoparticle system exhibited a Drude-like response.<sup>8</sup> Similar measurements on InP nanoparticles<sup>9</sup> could not be explained by a simple Drude conductivity behavior. However, a Drude-Smith model, which included a parameter for the degree of carrier backscattering produced a satisfactory fit to the InP data.

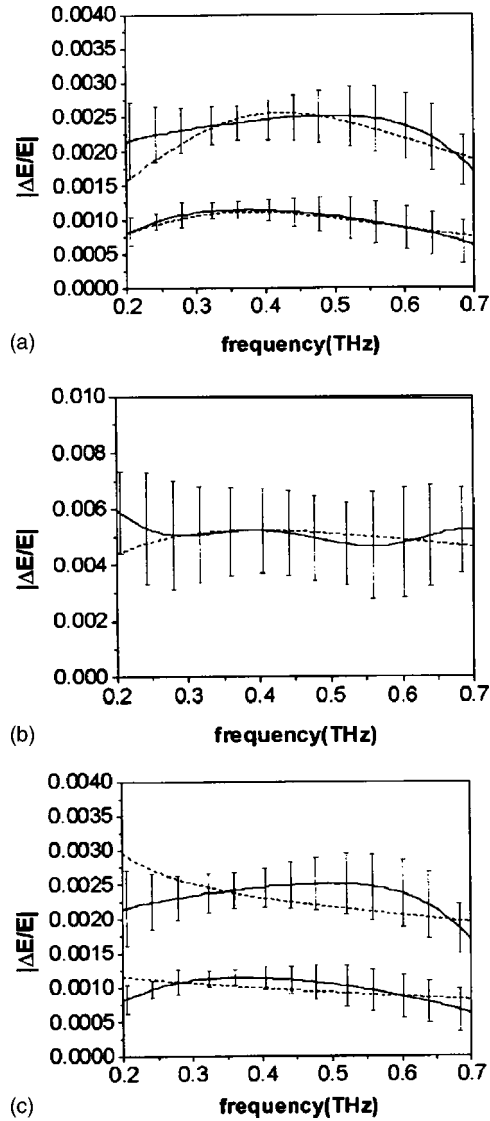


FIG. 4. Fits using both a Drude+Lorentz model to raw data differential transmission curves for (a) SWCNTs, (b) ion-implanted Si nanocrystals, and Drude only model for (c) SWCNTs. Bold lines are the raw data while the dashed lines are best fit curves; error bars show the fluctuation in the raw data due to noise as described in the analysis. Drude parameters for all fits were  $\tau=1E-11$  s,  $\Delta N=1E12$  cm<sup>-3</sup> for fits in (a) and (b) and  $\Delta N=1E18$  cm<sup>-3</sup> in (c), with Garnett parameter of  $1-X=0.05$ , for upper curve SWCNTs,  $1-X=0.02$  for lower curve SWCNTs, and  $1-X=0.05$  for ion-implanted Si (Lorentz parameters are given in Table I).

In analyzing the SWCNT and ion-implanted silicon data, we can model the presence of localized states<sup>7,19</sup> by incorporating a Lorentz-type contribution to the dielectric constant of the material. Since the unpumped transmission through our samples is featureless, we assume that the contribution to the differential transmission is due to photoexcited carriers only. One can approximate  $\epsilon(\omega)$  as  $\epsilon(\omega) + \Delta\epsilon$ , where  $\Delta\epsilon$  is due to the photoexcited carriers. In this model, the dielectric constant of the nanotubes can be expressed as

$$\Delta\varepsilon(\omega) = \frac{4\pi\Delta N e/m}{\omega(\omega + i/\tau)} - \sum_{m=1}^M \frac{\Omega_m^2}{(\omega^2 - \omega_m^2) + i\Gamma_m\omega}, \quad (2)$$

where  $\Delta N$ ,  $\Omega_m$ ,  $\omega_m$ ,  $\Gamma_m$ , and  $M$  are the photoexcited carrier density, quantum efficiency, resonant frequency, resonant width, and number of resonance, respectively. Of these parameters,  $\Delta N$  is estimated from the visible pump power density, assuming 1% of light being absorbed. Varying  $\tau$  and  $\Delta N$

over the range of  $10^{-15}$ – $10^{-10}$  s<sup>-1</sup> and  $10^8$ – $10^{14}$  cm<sup>-3</sup>, respectively, does not affect the curve fitting. The fits were mostly sensitive to the Lorentz parameters but not to the Drude model parameters. Using Eq. (2) for the dielectric constant of the nanoparticles, the differential THz transmission through the sample can be modeled. Assuming a double layer with nanocomposite on a quartz substrate, one can write the transmission of the electric field at normal incidence in the form<sup>20</sup>

$$\frac{E}{E_o} = \frac{8n_s n_n e^{i(n_s-1)k_o L}}{(n_s + n_n)(1 + n_n) - e^{i2n_s L k_o} [(n_n - n_s)(1 - n_n)] / [(n_n + n_s)(n_n + 1)]}, \quad (3)$$

where  $n_s$  is the index of refraction of the substrate,  $n_n$  and  $L$  are the index of refraction and thickness of the nano layer, and  $k_o = c/\omega$ , where  $c$  is the speed of light in a vacuum. For our experimental configuration, the THz differential signal is proportional to  $\Delta E = E_p - E_u$ , where  $E_p$  denotes the transmitted electric field through the material under optical illumination,  $E_u$  represents the electric field transmission without illumination, and  $E_o$  is the incident electric field. In the limit of a small photoinduced change in the nanotube's index of refraction [ $n_n = \sqrt{\varepsilon} = n_o + \Delta n$ , where  $\Delta n = (\Delta\varepsilon/2)\varepsilon_\infty$ ], the differential THz signal can be expressed using Eqs. (2) and (3) to first order in  $\Delta n$ ,

$$\frac{|\Delta E|}{|E_o|} = \left| \left[ 1 + \frac{\Delta n}{n_n} \right] \frac{[1 + ik_o L \Delta n] \alpha_o}{[(n_n + n_s + \Delta n)(1 + n_n + \Delta n)] - e^{i2n_s L k_o} [(n_n - n_s + \Delta n)(1 - n_n - \Delta n)] [1 + ik_o L \Delta n]} - 1 \right| \quad (4)$$

with

$$\alpha_o = [(n_n + n_s)(1 + n_n)] - [(n_n - n_s)(1 - n_n)] e^{i2n_s L k_o}. \quad (5)$$

The analysis may be simplified if reflections from the front and back surface of the substrate are neglected. This is justified since time window is in a very narrow time region around the pulse so that reflections are not “seen” in our time window. Reflections from the front and back surfaces of the nanofilm are included in the calculation. In addition, we apply Garnett theory which describes an effective dielectric constant for conductive (or doped semiconductive) particles embedded in a dielectric layer.<sup>21</sup> This model is applicable to our samples since transmission electron microscopy measurements showed that both the SWCNTs and Si nanoclusters were well separated and statistically distributed, implying that the dc conductivity was negligible. We treat the ion-implanted Si nanocrystals as embedded particles in the quartz substrate and the SWCNTs as embedded in a layer of air on top of quartz. In this model the dielectric constant is represented as

$$\frac{\varepsilon - \varepsilon_i}{\varepsilon + 2\varepsilon_i} = (1 - X) \frac{\varepsilon_n - \varepsilon_i}{\varepsilon_n + 2\varepsilon_i}, \quad (6)$$

where  $\varepsilon$ ,  $\varepsilon_n$ ,  $\varepsilon_i$  are dielectric constants for the effective nanolayer, the nanomaterial itself, and the insulator, respectively.  $1 - X$  represents the fraction of nanomaterial in that effective layer. Using Eqs. (4) and (6), the Lorentz parameters (Table I) are extracted from the differential spectra. In Fig. 4, the Fourier transform of the raw data is compared to the Lorentz fits.

## V. DISCUSSION

Differential transmission in the frequency domain proved useful when analyzing THz transmission under delayed pump beam. The optically generated carriers respond to the probing THz radiation and, therefore, modify the THz transmission in the visible pump-THz probe geometry. Both SWCNTz and ion-implanted samples, which were used in our experiments, exhibit nonlinear characteristics of short-lived photoinduced carriers.<sup>16,17</sup>

Initially, in the case of the ion-implanted silicon, we compared the data to what we would expect from bulk semiconductors. The differential transmission spectra of the bulk semiconductor silicon [Fig. 3(b)] can be fit using only a free-carrier Drude model. Similarly other bulk semiconductors such as InP (Ref. 9) also exhibited photoinduced Drude-like behavior. The differential transmission data for our nanocomposite samples clearly indicate the necessity for a model beyond the Drude only or Drude-Smith model. A simple free-carrier dispersion model could not explain the large signal observed with our samples when pumped with relatively low pump intensities (<10 nJ) and when assuming accepted dc conductivity and electron mobility values.<sup>22</sup>

Given these values, to be able to fit the observed differ-

TABLE I. Extracted Lorentz parameters from differential THz spectra.

	$M$	$\omega_o$ (cm <sup>-1</sup> ) <sup>a</sup>	$\Omega_m$ (cm <sup>-1</sup> )	$\Gamma_m$ (cm <sup>-1</sup> )
SWCNT	1	16	1180	130
3–4 nm Ion Implanted Si	1	18	1420	260

<sup>a</sup>33 cm<sup>-1</sup> = 1 THz.

ential transmission with the Drude model, the photoinduced carrier density for a single 100 fs pulse would need to be  $\sim 10^{18} \text{ cm}^{-3}$  (compared to  $10^{12} \text{ cm}^{-3}$  as with the Drude + Lorentz model) in order to produce the experimentally observed  $|\Delta E/E|$  ratio of  $\sim 10^{-3}$  [Fig. 4(c)]. The required photoinduced carrier density would therefore correspond to a photoexcitation energy value of 4 mJ in our experiments. Given that the spot size of our pump beam, laser repetition rate, pulse duration, and thickness of the nanolayer were 1 cm, 82 MHz, 100 fs, and 100 nm, respectively, a value of 4 mJ is orders of magnitude larger than the actual experimental pulse energy values (estimated at 4 nJ in our experiment). For this estimation to hold, it was assumed that 1% of the pump light was absorbed and that one electron-hole pair was generated for each photon of the pump beam. As with the Drude model, when the Drude-Smith model<sup>9</sup> was considered the carrier density and consequential, required pump power levels were orders of magnitude larger than those used in our experiments. Our motivation for applying the Drude + Lorentz model lies in the fact that Lorentz-like states have been observed for SWCNT samples with relatively large oscillator strengths<sup>23</sup> from 30 to 12 000  $\text{cm}^{-1}$ .

Figure 4(a) shows the SWCNT data modeled with a single Lorentz state. The relatively large oscillator strength (1180  $\text{cm}^{-1}$ ) and width (130  $\text{cm}^{-1}$ ) of the Lorentz state are consistent with Lorentz-like states that were observed in linear spectroscopic measurements. Moreover, density variations of nanotubes on the sample [Figs. 2(a), 2(b), and 4(a)] do not affect the general shape of the response as observed with the THz probe. While the differential spectra shape of a Drude-Smith model would be similar to the spectral shape of the Lorentz fit of Fig. 4(a), the required pump power and photoinduced carrier density to reproduce the experimentally observed  $|\Delta E/E|$  strongly suggests that the Drude-Smith model is not the appropriate approach.

The ion-implanted differential spectrum of Fig. 4(b) was fit using one Lorentz state as shown in Table I. Also, we could not rule out the possibility that the flat differential spectrum is the tail of spectrally broadened Lorentz state whose center frequency lies outside of our 0.2–0.7 THz spectral band.

The values for  $\tau$  in the analysis assumes that the semiconducting nanotubes have mobilities of about 20,000  $\text{cm}^2/\text{V s}$  corresponding to  $\tau = 1\text{E-}11$  s. The evidence that these states were exhibited only under visible pumping should not be a surprise considering the mechanisms that has been discussed in the literature.<sup>24,25</sup> Quantum models suggested that when the scale of the structured material is on the order of the mean-free path, the energy distribution could be quantized into discrete states. Semiconducting carbon nanotubes differ from metallic ones by their chirality, both exhibiting different properties in the THz regime.<sup>7,19</sup> For the former, intraband transition energies have been shown to lie in the low frequency THz range, and scale inversely with the diameter of the tube.<sup>26</sup>

## VI. CONCLUSION

In summary, with the use of a noncontact visible pump-THz probe technique, the differential THz spectra of SWCNTs and ion-implanted Si nanoclusters exhibited the existence of photoinduced states. A photoinduced free-carrier Drude or Drude-Smith model was not consistent with the magnitude of the transmission value changes. A better fit was obtained when incorporating Lorentzian-like discrete states. The SWCNT data were consistent with a single Lorentz state in the measured frequency range. The flatness of the ion-implanted Si nanocluster spectra indicated either the presence of a broad Lorentz state in the 0.2–0.7 THz range or the presence of a much broader Lorentz peak outside our spectral range.

## ACKNOWLEDGMENT

The support of the U.S. Army Research Office (Contract No. DAAD 19-01-1-0009) is gratefully acknowledged.

- <sup>1</sup>S. Iijima and T. Ichihashi, *Nature (London)* **363**, 603 (1993).
- <sup>2</sup>M. S. Dresselhaus, G. Dresselhaus, and P. C. Eklund, *Science of Fullerenes and Carbon Nanotubes* (Academic, New York, 1996).
- <sup>3</sup>A. Thess *et al.*, *Science* **273**, 483 (1996).
- <sup>4</sup>A. Lan, Z. Iqbal, A. Aitouchen, M. Libera, and H. Grebel, *Appl. Phys. Lett.* **81**, 433 (2002).
- <sup>5</sup>M. Ajgaonkar, Y. Zhang, H. Grebel, and R. A. Brown, *J. Opt. Soc. Am. B* **19**, 1391 (2002).
- <sup>6</sup>O. Hilt, H. B. Brom, and M. Ahlsgog, *Phys. Rev. B* **61**, R5129 (2000).
- <sup>7</sup>J. Han, Z. Zhu, Y. Liao, Z. Wang, L. Yu, W. Zhang, L. Sun, and T. Wang, *JETP Lett.* **78**, 904 (2003).
- <sup>8</sup>M. C. Beard, G. M. Turner, and C. A. Schmittenmaer, *Nano Lett.* **2**, 983 (2002).
- <sup>9</sup>M. C. Beard, G. M. Turner, J. E. Murphy, O. I. Micic, M. C. Hanna, A. J. Nozik, and C. A. Schmittenmaer, *Nano Lett.* **3**, 1695 (2003).
- <sup>10</sup>M. van Exter and D. Grischowsky, *Appl. Phys. Lett.* **56**, 1694 (1990).
- <sup>11</sup>P. Saeta, J. F. Federici, B. I. Greene, and D. R. Dykaar, *Appl. Phys. Lett.* **60**, 1477 (1992).
- <sup>12</sup>S. S. Prabhu, S. E. Ralph, M. R. Melloch, and E. S. Harmon, *Appl. Phys. Lett.* **70**, 2419 (1997).
- <sup>13</sup>M. C. Beard, G. M. Turner, and C. A. Schmittenmaer, *J. Appl. Phys.* **90**, 5915 (2001).
- <sup>14</sup>H. Grebel, Z. Iqbal, and A. Lan, *Chem. Phys. Lett.* **348**, 203 (2001).
- <sup>15</sup>T. Jeon, K. Kim, C. Kang, S. Oh, J. Son, K. H. An, D. J. Bae, and Y. H. Lee, *Appl. Phys. Lett.* **80**, 3403 (2002).
- <sup>16</sup>H. Han, S. Vijayalakshmi, A. Lan, Z. Iqbal, H. Grebel, E. Lalanne, and A. M. Johnson, *Appl. Phys. Lett.* **82**, 1458 (2003).
- <sup>17</sup>S. Vijayalakshmi, H. Grebel, G. Yaglioglu, R. Pino, R. Dornsville, and C. W. White, *J. Appl. Phys.* **88**, 6418 (2000).
- <sup>18</sup>H. Altan, F. Huang, J. Federici, A. Lan, and H. Grebel, *Proc. SPIE* **5070**, 53 (2003).
- <sup>19</sup>A. Ugawa, A. G. Rinzier, and D. B. Tanner, *Phys. Rev. B* **60**, R11305 (1999).
- <sup>20</sup>M. Born and E. Wolfe, *Principles of Optics*, 7th ed. (Cambridge University Press, New York, 1999).
- <sup>21</sup>R. W. Cohen, G. D. Cody, M. D. Coutts, and B. Abeles, *Phys. Rev. B* **8**, 3689 (1973).
- <sup>22</sup>T. Dürkop, S. A. Getty, E. Corbas, and M. S. Fuhrer, *Nano Lett.* **4**, 35 (2004).
- <sup>23</sup>F. Borondics, K. Kamaras, Z. Chen, A. G. Rinzier, M. Nikolou, and D. B. Tanner, *XVIIth International Winter School on Electronic Properties of Novel Materials*, 2003.
- <sup>24</sup>A. L. Efros, *Sov. Phys. Semicond.* **16**, 772 (1982).
- <sup>25</sup>L. E. Brus, *J. Chem. Phys.* **80**, 4403 (1984).
- <sup>26</sup>A. Ugawa, J. Hwang, H. H. Gommans, H. Tashiro, A. G. Rinzier, and D. B. Tanner, *Curr. Appl. Phys.* **1**, 45 (2001).